Pergamon

Int. J. Heat Mass Transfer. Vol. 39, No. 16, pp. 3417–3423, 1996

0017-9310/96 $15.00 + 0.00

0017-9310(95)00408-4

Thermal effects on the morphological stability in a directional solidification system with remote flow

CHI-CHUAN HWANG, JIN-YUAN HSIEH and CHIN-CHAN CHUAN

Department of Mechanical Engineering, Chung Yuan University, Chung Li, Taiwan 32023, Republic of China

(*Received* 21 *April* 1995 *and in final form* 20 *November* 1995)

Abstract—In this paper we investigate the effect of thermal fields on the morphological stability in a directional solidification system with remote flow. We undertake a linear analysis and develop an asymptotic solution for large Schmidt number. The result shows that the system is more stable when the latent heat increases and/or the ratio of conductivity of solid to that of melt gets smaller. The lead/tin alloy is taken for a realistic example and the result shows that the freezing lead/tin system is more stable when the thermal effect is taken into consideration. Copyright © 1996 Elsevier Science Ltd.

INTRODUCTION

In recent decades, solidification of dilute binary alloys has been studied extensively, because it is the main method by which electronic materials are produced. During the solidification process, the planar, solid–liquid interface may become unstable to a cellular structure [1–3], resulting in unwanted compositional inhomogeneities in the solidified material. This is known as the morphological instability.

The first explanation of the morphological instability was given by Tiller *et al.* [4] in terms of the mechanism of constitutional supercooling. Mullins and Sekerka [5] first adopted the infinite one-sided model by neglecting the solute diffusion in the solid to establish the linear theory. Wollkind and Segel [6] and Wollkind *et al.* [7] extended the theory to the weakly nonlinear regime.

Fluid motion within the melt is known to have considerable influence on the stability of the system and has been the subject of reviews by Coriell and Sekerka [8] and Glicksman *et al.* [9]. The effect of model force flows, representing large scale fluid motions in the melt, on the morphological stability of the solid–liquid interface has been considered analytically by Delves [10, 11] for Blasius and quadratic flow profiles, and numerically by Coriell *et al.* [12] for a Couette flow. In both cases a linear stability analysis was employed which predicted some stabilization of the morphological instability for disturbances with wave vectors in the direction of fluid flow. Brattkus and Davis [13] conducted a weakly nonlinear analysis for a model flow representing the solidification of a rotating disk. They found that the flow over the interface induced by rotation promotes a long-wave instability. Brattkus and Davis [14] and McFadden *et al.* [15] have considered the effect of a planar stagnation-point flow. In particular Brattkus and Davis [14] found a destabilization of the system for long-wavelength disturbances which are found to propagate in the opposite direction to the direction of the flow. McFadden *et al.* [15] conducted a numerical investigation of this situation and predicted the flow to have a stabilizing effect on the morphological stability of the system.

Forth and Wheeler [16] investigated the interaction of the morphological mode of instability of a planar interface with the hydrodynamic, shear mode of instability due to the presence of a model boundary-layer flow adjacent to the interface. They adopted the asymptotic-suction-profile flow velocity, because it has the advantage that it is an exact solution of the Navier–Stokes equations which can avoid making the bound-layer approximation as was done by Delves [10, 11]. Forth and Wheeler [16] further used the frozen-temperature approximation, which decouples the temperature field from the solute field by assuming equal thermal conductivities in the solid and liquid phases, zero latent heat release at the interface, and the solute diffusivity is much less than heat diffusivity.

However, one would expect that the frozen-temperature approximation will lose accuracy at higher pulling speeds because of the large amount of latent heat released. In this work, we would like to improve the accuracy of Forth and Wheeler's results [16] by taking the thermal effect into consideration. The governing equations of the present problem to be considered will be described, accompanied with suitable boundary conditions, in the next section. The basic solution to these equations is then obtained in this same section. As the basic solution is obtained, a linear stability analysis will be undertaken. Small perturbations are added to the basic solution and the Orr–Sommerfeld equation of these perturbations is

NOMENCLATURE

C_∞	far-field concentration
C	non-dimensional solute concentration
$\hat{c}$	wave speed
D	differential operator (d/dz)
$\tilde{D}$	solute diffusion coefficient
G_c	non-dimensional concentration gradient at the interface
G_L	non-dimensional temperature gradient of liquid
G_S	non-dimensional temperature gradient of solid
K	non-dimensional curvature of the interface
L	latent heat per unit volume
m	liquidus slope
M	non-dimensional liquidus slope
$\hat{\mathbf{n}}$	unit vector normal to the interface direction towards the fluid
n_c	conductivity ratio, κ_S/κ_L
n_d	diffusivity ratio, α_S/α_L
p	non-dimensional pressure
Pr	Prandtl number in liquid, v/α_L
Re	Reynold number, U_∞^*/V_0^*
S	inverse Sekerka number, $1/S_k$
Sc	Schmidt number, $v/\tilde{D}$
Sk	Sekerka number, MG_c/G_L
t	non-dimensional time
T_L	non-dimensional temperature in the liquid
T_S	non-dimensional temperature in the solid
u	non-dimensional velocity
U_∞	far-field velocity
T_m	temperature at melting point
T_i	interfacial temperature
V_0	growth speed
x, y, z	non-dimensional spatial coordinate
$\hat{\mathbf{z}}$	unit vector in the z-direction.

Greek symbols

$\hat{\alpha}$	wavenumber in the x-direction
α_L	thermal diffusivity of liquid
α_S	thermal diffusivity of solid
$\hat{\beta}$	wavenumber in the y-direction
$\hat{\gamma}$	wavenumber, $\sqrt{\hat{\alpha}^2+\hat{\beta}^2}$
κ_L	thermal conductivity of liquid
κ_S	thermal conductivity of solid
κ	partition coefficient
μ	non-dimensional capillarity parameter
v	kinematics viscosity of the fluid
ρ	density of the fluid.

Superscript

*	dimensional quantity.

obtained. We will solve the Orr–Sommerfeld equation after expanding all of the variable into a power series of the inverse Schmidt number and will obtain the asymptotic solution. Results so obtained will be compared with those obtained by Forth and Wheeler [16]. In the last section we will draw a brief conclusion.

THE GOVERNING EQUATIONS

In this work, we consider a dilute binary alloy freezing at a solid liquid interface when a temperature gradient is present. The liquid phase is in motion with a non-zero component of velocity parallel to the solid–liquid interface. In both the theoretical and the practical sense, the interface is rationally assumed to be planar at the first stage and to advance into the fluid with an average speed V_0^*. We locate our coordinate system in a frame of reference coincident with the average position of the interface, which is given by $z^* = 0$. The fluid is assumed to be of semi-infinite extent and to occupy the region $z^* > 0$. The free-stream velocity and solute concentrations are prescribed in the liquid phase far from the interface and can be considered to represent the behavior of large scale transport processes in a real crystal-growth melt. Figure 1 shows the physical configuration described above.

We are concerned here with the interaction of the morphological instability of the interface under the effects of both the fluid flow and the fluctuation of the temperature gradient, and therefore neglect the effect of gravity. To neglect the convective effect of the melt, we assume there is no change of density of the alloy on solidification. For most semiconducting alloys the diffusion coefficient of solute in the solid is several orders of magnitude smaller than that of the liquid phase, hence we assume that the effect of diffusion in the solid phase is negligible. Further we assume that the liquid is incompressible and that the alloy is dilute.

Under the above assumptions the Navier–Stokes equations and convection–diffusion equation govern the transport of momentum, solute, and thermal heat, respectively. Hence, we have

$$\frac{\partial u^*}{\partial t^*} + u^* \cdot \nabla u^* = \frac{-1}{\rho}\nabla p^* + v\nabla^2 u^* \tag{1}$$

$$\frac{\partial C^*}{\partial t^*} + u^* \cdot \nabla C^* = \tilde{D}\nabla^2 C^* \tag{2}$$

$$\frac{\partial T_L^*}{\partial t^*} + u^* \cdot \nabla T_L^* = \alpha_L \nabla^2 T_L^* \tag{3}$$

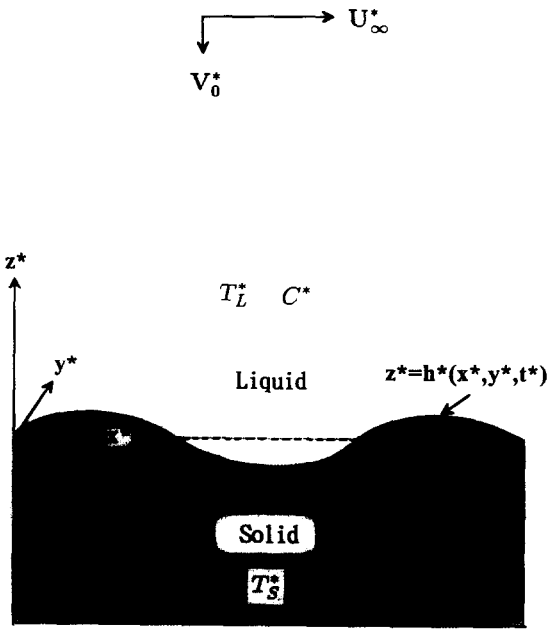

Fig. 1. The physical configuration of a freezing alloy.

$$\frac{\partial T_S^*}{\partial t^*} - V_0^* \frac{\partial T_S^*}{\partial z^*} = \alpha_S \nabla^2 T_S^* \tag{4}$$

and the assumption of incompressible flow yields

$$\nabla \cdot u^* = 0 \tag{5}$$

where u^*, p^*, c^* are the dimensional velocity, pressure and solute concentration, respectively, T_L^* and T_S^* are dimensional temperature in the liquid and the solid phases, respectively, α_L and α_S represent the thermal diffusion coefficients in the liquid and solid phases, respectively, ν and ρ are the kinematics viscosity and density of the fluid, $\tilde{D}$ is the solute diffusion coefficient in the liquid phase, and V_0^* is the pulling rate of the growing alloy

The boundary conditions at the solid–liquid interface, which we describe by $z = h^*(x^*, y^*, t^*)$, are

$$(u^* + V_0^* \hat{\mathbf{z}}) \cdot \hat{\mathbf{n}} = 0 \tag{6}$$

$$(u^* + V_0^* \hat{\mathbf{z}}) \times \hat{\mathbf{n}} = 0 \tag{7}$$

$$\tilde{D} \nabla C^* \cdot \hat{\mathbf{n}} = (k-1) C^* (V_0^* \hat{\mathbf{z}} + V_b^*) \cdot \hat{\mathbf{n}} \tag{8}$$

$$T^* = T_m^* + mC^* + T_m^* \mu^* K^* \tag{9}$$

$$L^* V_0^* \hat{\mathbf{z}} \cdot \hat{\mathbf{n}} = (-k_L \nabla T_L^* + k_S \nabla T_S^*) \cdot \hat{\mathbf{n}} \tag{10}$$

$$T_S^* = T_L^* = T_i^* \tag{11}$$

Equation (6) describes the conservation of mass at the interface, where $\hat{\mathbf{n}}$ is the unit vector normal to the interface directed towards the fluid, $\hat{\mathbf{z}}$ is the unit vector in the z^*-direction. Equation (7) is the no-slip condition. Equation (8) expresses the conservation of solute across the interface, where k is known as the segregation coefficient and V_b^* is the velocity of the solid–liquid interface in our moving frame of reference. Equation (9) describes the dependence of the freezing temperature of a binary alloy upon its composition and also, in its last term, includes the capillarity effects referred to as the Gibbs–Thompson effect. In equation (9), T_m^* is the freezing temperature of the pure substance, m the liquidus slope, μ^* is the capillarity constant, and K^* is the curvature of the interface. Equation (10) is the conservation of energy across the interface, where L^* denotes the latent heat, k_L and k_S are thermal conductive coefficients in the liquid and solid phase, respectively. The last boundary condition expresses the continuity of temperature across the interface, where T_i^* is the interfacial temperature.

The far-field boundary conditions are

$$u^* \to (U_\infty^*, 0, -V_0^*) \tag{12}$$

$$C^* \to C_\infty^* \tag{13}$$

$$\frac{\partial T_L^*}{\partial z^*} \to G_L^* \exp\left(-\frac{V_0^*}{\alpha_L} z^*\right) \tag{14}$$

$$\frac{\partial T_S^*}{\partial z^*} \to G_S^* \exp\left(-\frac{V_0^*}{\alpha_S} z^*\right) \tag{15}$$

as $z^* \to \infty$. Here G_L^* and G_S^* denote the temperature gradient in the liquid and solid phase at planar interface ($z^* = 0$), respectively.

Thus a steady-state solution to equations (1)–(5) with boundary conditions (6)–(15) is

$$U_0^*(z^*) = U_\infty^* \left[1 - \exp\left(\frac{-V_0^* z^*}{\nu}\right)\right] \tag{16}$$

$$C_0^*(z^*) = C_\infty^* \left[1 + \frac{1-k}{k} \exp\left(\frac{-V_0^* z^*}{\tilde{D}}\right)\right] \tag{17}$$

$$T_{L0}^*(z^*) = T_m^* + mC_0^*(0) + \frac{\alpha_L}{V_0^*} G_L^* \left[1 + \exp\left(\frac{-V_0^* z^*}{\alpha_L}\right)\right] \tag{18}$$

$$T_{S0}^*(z^*) = T_m^* + mC_0^*(0) + \frac{\alpha_S}{V_0^*} G_S^* \left[1 - \exp\left(\frac{-V_0^* z^*}{\alpha_S}\right)\right] \tag{19}$$

$$p_0^*(\mathbf{x}^*) = p_0^*. \tag{20}$$

We shall non-dimensionalize the problem by putting

$$\mathbf{x}^* = (\tilde{D}/V_0^*)\mathbf{x} \quad u^* = V_0^* u$$

$$t^* = (\tilde{D}/V_0^{*2})t \quad p^* = \rho V_0^{*2} p$$

$$T^* = T_m^* T \quad C^* = C_\infty^* C \quad h^* = (\tilde{D}/V_0^*) h(x, y, t)$$

$$G_L^* = \frac{T_m^* G_L}{(\tilde{D}/V_0^*)} \quad G_S^* = \frac{T_m^* G_S}{(\tilde{D}/V_0^*)} \tag{21}$$

in which the dimensional governing equations (1)–(5) are transformed into the non-dimensional ones

$$\frac{\partial u}{\partial t}+u\cdot\nabla u=-\nabla p+Sc\nabla^2 u \tag{22}$$

$$\frac{\partial C}{\partial t}+u\cdot\nabla C=\nabla^2 C \tag{23}$$

$$\frac{Pr}{Sc}\frac{\partial T_L}{\partial t}-\frac{Pr}{Sc}(u\cdot\nabla T_L)=\nabla^2 T_i \tag{24}$$

$$\frac{Pr}{Sc}\frac{\partial T_S}{\partial t}-\frac{Pr}{Sc}\frac{\partial T_S}{\partial z}=n_d\nabla^2 T_S \tag{25}$$

$$\nabla\cdot u=0 \tag{26}$$

where $Sc=\nu/\tilde{D}$ is the Schmidt number, $Pr=\nu/\alpha_L$ is the Prandtl number and $n_d=\alpha_S/\alpha_L$.

The corresponding nondimensional boundary conditions at the solid–liquid interface $z=h(x,y,t)$ are

$$(u+\hat{\mathbf{z}})\cdot\hat{\mathbf{n}}=0 \tag{27}$$

$$(u+\hat{\mathbf{z}})\times\hat{\mathbf{n}}=0 \tag{28}$$

$$\nabla C\cdot\hat{\mathbf{n}}=(k-1)C(\hat{\mathbf{z}}+V_0)\cdot\hat{\mathbf{n}} \tag{29}$$

$$T=1+MC+\mu K \tag{30}$$

$$L\hat{\mathbf{z}}\cdot\hat{\mathbf{n}}=(-\nabla T_L+n_r\nabla T_S)\cdot\hat{\mathbf{n}} \tag{31}$$

and

$$T_S=T_L=T_i \tag{32}$$

where

$$M=mC_\infty^*/T_m^* \quad \mu=\mu^* V_0/\tilde{D}$$
$$L=L^*\tilde{D}/k_l T_m^* \quad n_r=k_l/k_S \tag{33}$$

and K is the non-dimensional curvature of the interface.

We define a Reynolds number Re by

$$Re=U_\infty^*/V_0^* \tag{34}$$

so the far-field boundary conditions are in the following non-dimensional forms:

$$u\to(Re,0,-1) \tag{35}$$

$$C\to 1 \tag{36}$$

$$\partial T_L/\partial z=G_L\exp(-Prz/Sc) \tag{37}$$

$$\partial T_S/\partial z=G_S\exp(-Prz/n_d Sc). \tag{38}$$

The steady-state solutions (16)–(20) then become

$$u_0(\mathbf{x})=(U_0(z),0,-1) \tag{39}$$

where

$$U_0(z)=Re[1-\exp(-z/Sc)] \tag{40}$$

and

$$C_0(z)=1-G_c\exp(-z) \tag{41}$$

$$T_{L0}(z)=1+MC_0(0)+(Sc/Pr)G_L[1-\exp(-Prz/Sc)] \tag{42}$$

$$T_{S0}(z)=1+MC_0(0)+(n_d Sc/Pr)G_S[1-\exp(-Prz/n_d Sc)] \tag{43}$$

$$p_0(\mathbf{x})=p_0 \tag{44}$$

where

$$G_c=C_0'(0)=(k-1)/k. \tag{45}$$

LINEAR STABILITY ANALYSIS

We proceed to the linear stability analysis of the steady-state solutions by adding to them small perturbations such as

$$u(\mathbf{x},t)=(U_0(z)+\tilde{u}(\mathbf{x},t),\tilde{v}(\mathbf{x},t),-1+\tilde{w}(\mathbf{x},t)) \tag{46}$$

$$C(\mathbf{x},t)=C_0(z)+\tilde{c}(\mathbf{x},t) \tag{47}$$

$$T_L(\mathbf{x},t)=T_{L0}(z)+\tilde{T}_L(\mathbf{x},t) \tag{48}$$

$$T_S(\mathbf{x},t)=T_{S0}(z)+\tilde{T}_S(\mathbf{x},t) \tag{49}$$

$$p(\mathbf{x},t)=p_0+\tilde{p}(\mathbf{x},t) \tag{50}$$

$$h=\tilde{h}(x,y,t) \tag{51}$$

where

$$(\tilde{u},\tilde{v},\tilde{w},\tilde{c},\tilde{T}_L,\tilde{T}_S,\tilde{p})(\mathbf{x},t)=(\bar{u},\bar{v},\bar{w},\bar{c},\bar{T}_L,\bar{T}_S,\bar{p})(z)\exp[i\hat{\alpha}(x-\hat{c}t)+i\hat{\beta}y] \tag{52}$$

$$\tilde{h}(x,y,t)=\delta\exp[i\hat{\alpha}(x-\hat{c}t)+i\hat{\beta}y] \tag{53}$$

$\hat{\alpha}$ and $\hat{\beta}$ are the wavenumbers in the x- and y-directions, respectively, and $\hat{c}$ is the wave speed.

Now, linearizing the governing equations (22)–(26) and using the normal mode solutions (52)–(53) one can obtain

$$[Sc(D^2-\hat{r}^2)+D+i\hat{\alpha}(\hat{c}-U_0(z))]\bar{u}(z)=\bar{w}(z)DU_0(z)+i\hat{\alpha}\bar{p}(z) \tag{54}$$

$$[Sc(D^2-\hat{r}^2)+D+i\hat{\alpha}(\hat{c}-U_0(z))]\bar{v}(z)=i\hat{\beta}\bar{p}(z) \tag{55}$$

$$[Sc(D^2-\hat{r}^2)+D+i\hat{\alpha}(\hat{c}-U_0(z))]\bar{w}(z)=Dp(z) \tag{56}$$

$$i\hat{\alpha}\bar{u}(z)+i\hat{\beta}\bar{v}(z)+D\bar{w}(z)=0 \tag{57}$$

$$[(D^2-\hat{r}^2)+D+i\hat{\alpha}(\hat{c}-U_0(z))]\bar{C}(z)=\bar{w}(z)C_0'(z) \tag{58}$$

$$[D^2-\hat{r}^2]\bar{T}_L(z)=-i\hat{\alpha}\hat{c}(Pr/Sc)\bar{T}_L(z)-(Pr/Sc)[U_0(z)i\hat{\alpha}\bar{T}_L(z)-D\bar{T}_L(z)+\bar{w}(z)G_L\exp(-Prz/Sc)] \tag{59}$$

$$[D^2-\hat{r}^2]\bar{T}_S(z)=-i\hat{\alpha}\hat{c}(Pr/n_d Sc)\bar{T}_S(z)-(Pr/n_d Sc)D\bar{T}_S(z) \tag{60}$$

where D is the differential operator d/dz and

$\hat{r}^2 = \hat{\alpha}^2 + \hat{\beta}^2$. Using equation (57) to eliminate perturbed pressure $\bar{p}(z)$ yields

$$\{Sc(D^2-\hat{r}^2)^2 + [D + i\hat{\alpha}(\hat{c} - U_0(z))](D^2-\hat{r}^2) + i\hat{\alpha}D^2U_0(z)\}\bar{w}(z) = 0. \quad (61)$$

The boundary conditions at the perturbed interface (27) and (28) may be transferred to $z = 0$ yielding

$$\bar{w}(0) = 0 \quad (62)$$

$$\bar{u}(0) = -DU_0(0)\,\delta \quad (63)$$

and

$$\bar{v}(0) = 0. \quad (64)$$

Further equations (63) and (64) may be combined using equation (57) to give

$$D\bar{w}(0) = i\hat{\alpha}Re\,\delta/Sc \quad (65)$$

and equations (29)–(32) become

$$\delta G_c(i\hat{\alpha}\hat{c} - k) + D\bar{C}(0) - (k-1)\bar{C}(0) = 0 \quad (66)$$

$$\frac{\bar{C}(0)}{G_c} = \delta\left[\frac{1}{Sk} - 1 + \frac{\hat{\mu}\hat{r}^2}{MG_c}\right] + \frac{\bar{T}(0)}{MG_c} \quad (67)$$

$$+ i\hat{\alpha}\hat{c}L\,\delta = \left(G_L\frac{Pr}{Sc} - \frac{n_r}{n_d}G_S\frac{Pr}{Sc}\right)\delta + (-D\bar{T}_L(0) + n_rD\bar{T}_S(0)) \quad (68)$$

$$G_L\,\delta + \bar{T}_L(0) = G_S\,\delta + \bar{T}_S(0) \quad (69)$$

where Sk is the Sekerka number defined by $Sk = MG_c/G_L$.

The far-field boundary conditions then yield

$$\bar{w}(z), D\bar{w}(z), \bar{C}(z), \bar{T}_L(z) \to 0 \quad \text{as } z \to \infty \quad (70)$$

$$\bar{T}_S(z) \to 0 \quad \text{as } z \to -\infty \quad (71)$$

For given wavenumbers $\hat{\alpha}$ and $\hat{\beta}$, Reynolds number Re and Sekerka number Sk, as well as the parameters, k, Sc, $\hat{\mu}$, M, L, n_r, G_S and G_L, the equations (58)–(61), together with boundary conditions (62) and (65)–(70), define an eigenvalue problem for $\hat{c}$. Let $\hat{c}_i$ denote the imaginary part of $\hat{c}$, then the system is linearly stable if $\hat{\alpha}\hat{c}_i$ is negative for all wavenumbers; otherwise it is unstable.

STABILITY RESULTS SOLUTION FOR LARGE SCHMIDT NUMBER

Since the complete analytical solution is difficult to deduce, and since almost all alloys possess a large Schmidt number, we prefer to obtain an asymptotic one for large Schmidt number. Thus, in this paper we require that $Sc \to \infty$, Pr is $O(1/Sc)$, L is $O(1/Sc^2)$, and Re is $O(Sc^0)$. We therefore put the functions $\bar{w}(z)$, $\bar{c}(z)$, $\bar{T}_L(z)$ and $\bar{T}_S(z)$ into the asymptotic form

$$\phi(z) = \sum_{n=0}^{N} \phi_n(z)/Sc^n \quad (72)$$

where N is a positive integer. Now we introduce a new parameter, the inverse Sekerka number, which is defined by $S = 1/Sk$. The parameters $\hat{c}$, $S\,G_L$ and G_S are also put into asymptotic form

$$\psi = \sum_{n=0}^{N} \psi_n/Sc^n. \quad (73)$$

Then the governing equations (58)–(61), together with boundary conditions (62) and (65)–(70), are solved successively at each order of the small parameter $1/Sc$.

At each order, $\bar{w}_n(z)$, $\bar{C}_n(z)$, $\bar{T}_{Ln}(z)$ and $\bar{T}_{Sn}(z)$ are solved simultaneously and consequently one will obtain a dispersion relation, which describes the relation among the wave speed $\hat{c}_n$ and other control and material parameters. To study the curve of marginal stability, one simply lets the imaginary part of $\hat{c}_n$ be equal to zero and then have a relation, say, among S_n and other control and material parameters. In the present study, we continue the calculating procedure and stop at $O(1/Sc^2)$. So we have

$$S = S_0 + S_1/Sc + S_2/Sc^2 \quad (74)$$

where S_0, S_1 and S_2 satisfy the following relations:

$$\left[1 - \frac{n_r}{1+n_r}\left(1 - \frac{1}{n_r}\right)\right]S_0 = 1 - \frac{\hat{\mu}\hat{r}^2}{MG_c} - \frac{L}{MG_c}\frac{1}{1+n_r} - \frac{k}{k-\frac{1}{2}+R} \quad (75)$$

$$S_1 = i\hat{\alpha}\{\hat{c}_1 H(k,\hat{r}) - ReU(k,\hat{r})\} \quad (76)$$

and

$$\begin{aligned}(k-\tfrac{1}{2}+R)&\left[1 - \frac{n_r}{1+n_r}\left(1 - \frac{1}{n_r}\right)\right]S_2 \\ &= \hat{\alpha}^2Re^2\left\{-\frac{1}{\hat{r}^2}\left[\frac{1}{\hat{r}}(2\hat{r}+1)+1\right]\right. \\ &+ \frac{3}{2R^2}\cdot\frac{k}{k-\frac{1}{2}+R}\left[\frac{1}{16R^3} - \frac{H(k,\hat{r})}{24R^2}\right. \\ &\left. + \frac{1}{6R^2}\left(-\frac{H(k,\hat{r})}{2} + \frac{1}{4R}\right)\right] \\ &- \frac{H(k,\hat{r})}{4R^3}\left(-\frac{H(k,\hat{r})}{2} + \frac{1}{4R}\right)\frac{k}{k-\frac{1}{2}+R} \\ &- \frac{1}{R}\frac{1}{\hat{r}^2}(2\hat{r}+1)\left(\frac{1}{4R} - \frac{H(k,\hat{r})}{2}\right) \\ &+ (R-\hat{r}-\tfrac{1}{2})\left[\frac{1}{\hat{r}}(2\hat{r}+1)+1\right] \\ &\left.\times\left[-\frac{(2\hat{r}+1)}{\hat{r}^3} + \frac{H(k,\hat{r})}{\hat{r}^2}\right]\right\}\end{aligned}$$

$$-(k-\tfrac{1}{2}+R)\left\{\frac{S_0}{(1+n_r)\hat{r}}\left[\left(1-\frac{1}{n_r}\right)\right.\right.$$

$$\times\frac{n_r}{1+n_r}\frac{(n_d-1)Pr}{2}+(n_d-1)Pr\left.\right]$$

$$\left.+\frac{1}{(1+n_r)\hat{r}}\frac{L}{MG_c}\left[\frac{1}{1+n_r}\frac{(n_d-1)Pr}{2}-n_dPr\right]\right\}. \quad (77)$$

In equations (75)–(77), R, $H(k,\hat{r})$ and $U(k,\hat{r})$ are, respectively, expressed as

$$R=(\hat{r}^2+\tfrac{1}{4})^{1/2} \quad (78)$$

$$H(k,\hat{r})=\frac{1}{k-\frac{1}{2}+R}\left[1-\frac{k}{2R(k-\frac{1}{2}+R)}\right] \quad (79)$$

and

$$U(k,\hat{r})=\frac{1}{k-\frac{1}{2}+R}\left[\frac{(k+\hat{r})(2\hat{r}+1)}{\hat{r}^2}\right.$$

$$\left.-\frac{1}{\hat{r}}-\frac{k}{4R^2(k-\frac{1}{2}+R)}\right]-\frac{(2\hat{r}+1)}{\hat{r}^2}. \quad (80)$$

In equation (76), since on the marginal curve $\hat{c}_1$ is real, as are S_1, $\hat{\alpha}$, Re, $H(k,\hat{r})$ and $U(k,\hat{r})$, hence we must have

$$S_1=0 \quad (81)$$

and

$$\hat{c}_1=ReU(k,\hat{r})/H(k,\hat{r}). \quad (82)$$

It is known that a positive (negative) $\hat{c}_1$ represents a forward (backward)-traveling wave. Also we should keep in mind that, as $L=0$ and $n_r=1$, the present result will reduce to that Forth and Wheeler [16] have obtained.

In the following calculations, $Re=1$ is applied to perform the effect of the far-field fluid flow. As seen in equation (77), $|S_2|$ will be maximum when $\hat{\alpha}\equiv\hat{r}$, i.e. for modes parallel to the flow direction, so the calculations are undertaken under such consideration. Figure 2 shows the curves of marginal stability in the $(\hat{r},S)$ plane. In this figure, the effect of the latent heat on the morphological stability is shown. We see that as n_r is fixed, the freezing system is more stable as latent heat gets larger. The effect of the conductivity ratio, n_r, on the morphological stability is shown in Fig. 3. We see, in this figure, that the freezing system is more stable as the conductivity ratio gets smaller.

The overall thermal effect on the morphological stability is obviously the combination of the effects of the latent heat and of the conductivity ratio. We now take a lead/tin alloy as a realistic example for calculation. The realistic L/MG_c and n_r for lead/tin alloy are 0.8884 and 1.868, respectively. In Forth and Wheeler's study [16], they neglected the latent heat and assume the conductivity ratio is unity. The result is shown in Fig. 4. We can easily see that the realistic system of lead/tin alloy is more stable when the totally thermal effect is taken into consideration.

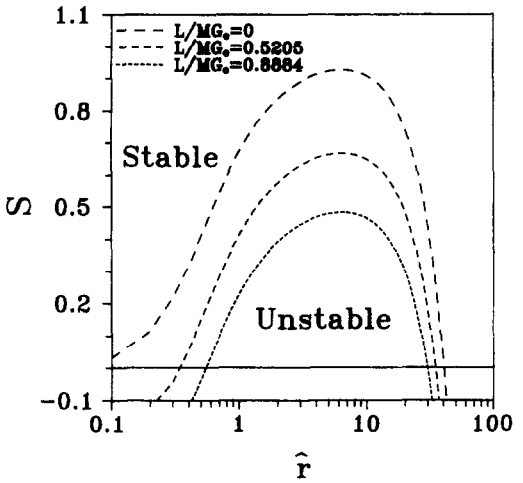

Fig. 2. Marginal stability curves with different value of L/MG_c in $(\hat{r},S)$ plane; $n_r=1.0$.

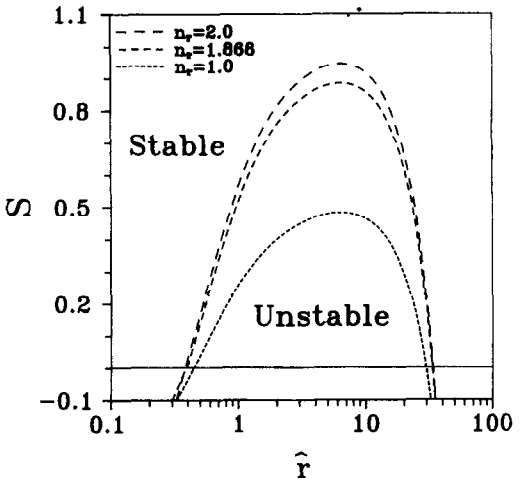

Fig. 3. Marginal stability curves with different value of n_r in $(\hat{r},S)$ plane; $L/MG_c=0.8884$.

CONCLUSION

In this work, we improve Forth and Wheeler's work [16] by taking the thermal effect into consideration. The linear result is obtained in an asymptotic form for large Schmidt number. The result shows that the system is more stable when the latent heat increases and/or the ratio of conductivity of solid to that of melt gets smaller. The lead/tin alloy is taken for a realistic consideration. The result shows that, when compared to Forth and Wheeler's, this realistic system is more stable when the thermal effects are taken into consideration.

Acknowledgement—The authors wish to acknowledge with appreciation the financial support (grant no. NSC 84-2212-

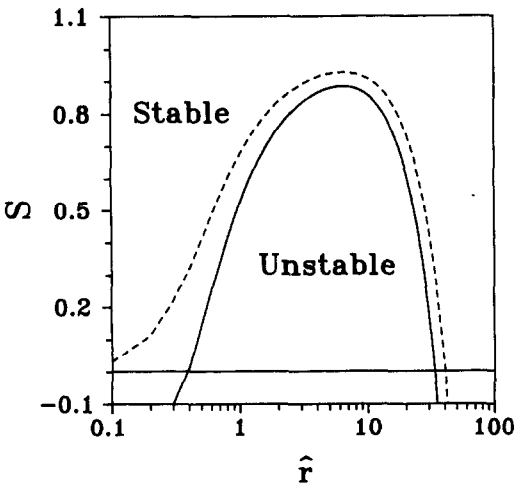

Fig. 4. Curves of marginal stability for a lead/tin alloy. The solid line represents the present analysis $n_r = 1.868$, $L/MG_c = 0.8884$); and the dashed one is from Forth and Wheeler [16] ($n_r = 1.0, L/MG_c = 0$).

E-033-002) provided by the National Science Council of the Republic of China.

REFERENCES

1. J. W. Rutter and B. Chalmers, A prismatic substructure formed during solidification of metals, *Can. J. Phys.* **31,** 15–39 (1953).
2. L. R. Morris and W. C. Winegard, The development of cells during the solidification of a dilute Pb–Sn alloy, *J. Crystal Growth* **5,** 361–375 (1969).
3. D. G. McCartney and J. D. Hunt, Measurement of cell and primary dendrite arm spacing in directionally solidified aluminum alloys, *Acta Metall.* **29,** 1851–1863 (1981).
4. W. A. Tiller, J. W. Rutter, K. A. Jackson and B. Chalmers, The redistribution of solute atoms during the solidification of metals, *Acta Metall.* **1,** 428–437 (1953).
5. W. W. Mullins and R. F. Sekerka, Stability of a planar interface during solidification of a dilute binary alloy, *J. Appl. Phys.* **35,** 444–451 (1964).
6. D. J. Wollkind and L. A. Segel, A nonlinear stability analysis of the freezing of a dilute binary alloy, *Phil. Trans. R. Soc. Lond.* **A268,** 351–380 (1970).
7. D. J. Wollkind, D. B. Outlon and R. Sriranganathan, A nonlinear stability analysis of a model equation for alloy solidification, *J. Phys. Paris* **45,** 505–516 (1984).
8. S. R. Coriell and R. F. Sekerka, Effect of convective flow on morphological stability, *J. Crystal Growth* **49,** 281–293 (1981).
9. M. E. Glicksman, S. R. Coriell and G. B. McFadden, Interaction of flows with the crystal–melt interface, *A. Rev. Fluid Mech.* **18,** 307–335 (1986).
10. R. T. Delves, Theory of a solid–liquid interface during growth from stirred melts, *J. Crystal Growth* **3,4** 562–568 (1968).
11. R. T. Delves, Theory of a solid–liquid interface during growth from stirred melts II, *J. Crystal Growth* **8,** 13–25 (1971).
12. S. R. Coriell, G. B. McFadden, R. F. Boisvert and R. F. Sekerka, Effect of a forced Couette flow on coupled convective and morphological instabilities during unidirectional solidification, *J. Crystal Growth* **69,** 15–22 (1984).
13. K. Brattkus and S. H. Davis, Flow induced morphological instabilities: the rotating disk, *J. Crystal Growth* **87,** 385–396 (1988).
14. K. Brattkus and S. H. Davis, Flow induced morphological instabilities: stagnation point flows, *J. Crystal Growth* **89,** 423–427 (1988).
15. G. B. McFadden, S. R. Coriell and J. I. D. Alexander, Hydrodynamic and free boundary instabilities during crystal growth: the effect of a plane stagnation point flow, *Appl. Maths.* **41,** 683–706 (1988).
16. S. A. Forth and A. A. Wheeler, Hydrodynamic and morphological stability of the unidirectional solidification of a freezing binary alloy: a simple model, *J. Fluid Mech.* **202,** 339–366 (1989).